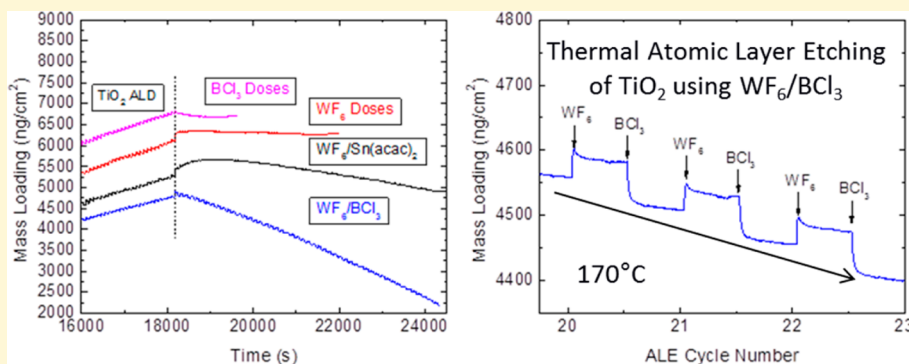


# Thermal Selective Vapor Etching of $\text{TiO}_2$ : Chemical Vapor Etching via $\text{WF}_6$ and Self-Limiting Atomic Layer Etching Using $\text{WF}_6$ and $\text{BCl}_3$

Paul C. Lemaire<sup>ID</sup> and Gregory N. Parsons<sup>\*ID</sup>

Department of Chemical & Biomolecular Engineering, North Carolina State University, Raleigh, North Carolina 27695, United States



**ABSTRACT:** Controlled thin film etching is essential for further development of sub-10 nm semiconductor devices. Vapor-phase thermal etching of oxides is appealing for achieving highly conformal etching of high aspect ratio features. We show that tungsten hexafluoride ( $\text{WF}_6$ ) can be used to selectively etch amorphous  $\text{TiO}_2$  films versus other oxides including  $\text{Al}_2\text{O}_3$ . Chemical vapor etching (CVE) of  $\text{TiO}_2$  by  $\text{WF}_6$  was studied with quartz crystal microbalance (QCM), spectroscopic ellipsometry, X-ray photoelectron spectroscopy (XPS), and thermodynamic modeling. The XPS results show evidence for a  $\text{WO}_x\text{F}_y$  layer that forms on the  $\text{TiO}_2$  films during the etch process, which may act as a surfactant layer to help enable fluorination of the  $\text{TiO}_2$ . Direct CVE of  $\text{TiO}_2$  by  $\text{WF}_6$  is strongly temperature dependent, where etching proceeds readily at 220 °C, but not at  $T \leq 170$  °C. This is consistent with thermodynamic modeling showing that the etching rate is determined by the volatilization of metal fluoride and  $\text{WF}_2\text{O}_2$  product species. We also show that, at low temperature,  $\text{BCl}_3$  can be used as a coreagent with  $\text{WF}_6$  to achieve self-limiting atomic layer etching (ALE) of  $\text{TiO}_2$ . At 170 °C, the rate of ALE saturates at ~0.6 Å/cycle, which is ~2× the rate of  $\text{TiO}_2$  ALD at the same temperature. Experimental QCM analysis shows selectivity for  $\text{TiO}_2$  ALE vs  $\text{Al}_2\text{O}_3$  as predicted by thermodynamic modeling. We also demonstrate and describe how etching reactions during initial cycles can differ from those during steady-state ALE, and we draw a physical analogy between rate evolution in ALE and well-known rate evolution during nucleation in atomic layer deposition (ALD). This work expands understanding of surface reactions in CVE and ALE and the range of reactants and materials that can be active for advanced thermal ALE processing.

## 1. INTRODUCTION

The semiconductor industry foresees multiple challenges in designing and manufacturing transistor devices for the 7 and 5 nm nodes. For example, standard patterning techniques, such as lithography, become much less applicable because of challenges maintaining edge definition and alignment to the underlying features. In addition, semiconductor devices typically utilize three-dimensional designs, creating complex high-aspect-ratio features. Accordingly, the semiconductor industry is looking toward controllable etching techniques to supplement currently used thin film deposition techniques.

Chemical vapor etching (CVE) of silicon (Si) native oxide is of interest to the semiconductor industry. Hydrogen fluoride (HF) liquid etching of Si native oxide<sup>1–3</sup> is ubiquitously utilized in the semiconductor industry, but in situ vapor etching helps limit the reformation of an interfacial oxide layer between Si and a deposited film.<sup>4–9</sup> For both solution and vapor phase etching,  $\text{H}_2\text{O}$  plays a significant role in HF etching of Si native

oxide, with significantly lower etch rates in anhydrous conditions.<sup>10–13</sup> In vapor phase etching, water creates a interfacial layer between the substrate and gas and acts as a proton donor and acceptor to catalytically activate the HF etch.<sup>2,11,12</sup> Although HF is a promising etchant, high HF concentrations can lead to uncontrolled etching.

Extending the anhydrous HF vapor etch to other oxides is often limited, because unlike  $\text{SiF}_4$ , many of the formed metal fluorides are nonvolatile at typical process temperatures and pressures.<sup>14</sup> Yet the nonvolatile product formation also creates an opportunity to create a more controlled etching process because the surface fluoride species passivate the substrate from additional fluorination. Surface fluorides or chlorides can then be removed anisotropically by a subsequent energy-enhanced

Received: March 9, 2017

Revised: July 3, 2017

Published: July 4, 2017

technique such as plasma exposure or  $\text{Ar}^+$  bombardment or plasma species. Ideally, the two individual steps are self-limiting, creating a process known as atomic layer etching (ALE). But even with large control over the bias and the energy of the species, it is possible to get uncontrolled etching or damage to sensitive features.<sup>15–18</sup>

In order to limit the issues that arise from energy-enhanced techniques, there is interest in purely thermally driven chemical ALE processes. Such techniques would enable conformal isotropic etching, which has many applications for etching in high aspect ratio structures.<sup>19</sup> There has been considerable work by George et al. studying selective etching of oxides using HF in combination with different metal coregents.<sup>20–23</sup> Specifically, HF was used to fluorinate metal oxides including  $\text{Al}_2\text{O}_3$ ,  $\text{HfO}_2$ , and  $\text{ZrO}_2$  creating a passivating metal fluoride layer.<sup>20–23</sup> Exposing the metal fluoride layer to a coreagent such as trimethylaluminum (TMA),<sup>20,23</sup> tin acetylacetone ( $\text{Sn}(\text{acac})_2$ ),<sup>20–22,24</sup> diethylaluminum chloride (DMAC),<sup>20</sup> or silicon tetrachloride ( $\text{SiCl}_4$ )<sup>20</sup> can lead to a ligand-exchange reaction. Depending on the metal fluoride and the extent of the ligand-exchange, the modified surface layer will be volatilized, reforming the original substrate surface termination. For example, an  $\text{AlF}_3$  surface layer is proposed to react with  $\text{Sn}(\text{acac})_2$  to form volatile  $\text{Al}(\text{acac})_3$  and  $\text{SnF}(\text{acac})_2$ .<sup>21,22</sup> This etching approach bears similarities to earlier work in which zinc oxide and copper were etched with hexafluoroacetone ( $\text{hHfac}$ )<sup>25</sup> and  $\text{hHfac}$  and  $\text{O}_3/\text{H}_2\text{O}_2$ <sup>26,27</sup> processes, respectively. Selective oxide etching has been achieved by adjusting the process temperature and selecting specific metal precursors that serve as ligand sources. For example, a HF/TMA ALE process was observed to etch  $\text{Al}_2\text{O}_3$  but not  $\text{ZrO}_2$  at 300 °C.<sup>20</sup> In place of HF, other chemicals could be considered for the surface modification step, such as  $\text{BCl}_3$ ,<sup>28</sup>  $\text{Cl}_2$ ,<sup>24,25</sup> and  $\text{WF}_6$ .

$\text{WF}_6$  is an appealing fluorinating agent and etchant. As a higher oxidation state covalently bound metal fluoride,  $\text{WF}_6$  is highly volatile at room temperature.<sup>30</sup> Tungsten is also among the most electronegative of the transition metals,<sup>31</sup> enabling selective fluoride transfer to other transition metals.<sup>30</sup> For example,  $\text{WF}_6$  was observed to undergo halogen exchange with  $\text{TiCl}_4$  and  $\text{BCl}_3$  but was considerably less reactive than  $\text{MoF}_6$ .<sup>30</sup> Yet despite being less reactive, fluorination of  $\text{TiO}_2$  with  $\text{WF}_6$  proceeds with a Gibbs free energy of  $-14.9$  kcal/mol, whereas HF fluorination is endothermic with  $\Delta G = 6.9$  kcal/mol. The thermodynamic fluorination step by HF may in part explain why other reported thermally driven ALE processes that utilize HF are unable to etch TiN.<sup>20</sup> In addition,  $\text{WF}_6$  has been observed to etch  $\text{SiO}_2$ <sup>32</sup> and  $\text{WO}_3$  films<sup>33</sup> and in an analogous system  $\text{NbCl}_5$  was observed to etch  $\text{Nb}_2\text{O}_5$ .<sup>34</sup>  $\text{WF}_6$  also has a zero net dipole moment, making it relatively easy to evacuate from a reaction chamber, an attractive feature for a cyclic ALE process. In contrast, HF is “stickier” because of its high dipole moment, which can lead to hydrogen bonding and long residence times.<sup>19</sup>

In this paper, we demonstrate that  $\text{WF}_6$  can be used as an etchant for controlled removal of  $\text{TiO}_2$  films in both chemical vapor etching and atomic layer etching sequences. We find that  $\text{WF}_6$  selectively etches  $\text{TiO}_2$  over  $\text{Al}_2\text{O}_3$ , which we ascribe to the ability of  $\text{TiO}_2$  to more readily form volatile products at low process temperatures. Using ex situ XPS analysis, we confirm  $\text{WF}_6$  etching of  $\text{TiO}_2$  films and provide evidence that etching proceeds through  $\text{TiO}_2$  fluorination in the film bulk and formation of a low density  $\text{WO}_x\text{F}_y$  surface layer on the etching film. Thinner  $\text{TiO}_2$  films require less time to become fully

fluorinated, resulting in overall more rapid chemical vapor etching than thicker  $\text{TiO}_2$  films.

We also find that by using a surface coupling agent the chemical etching via  $\text{WF}_6$  can be controlled to achieve a self-limiting ALE process. Specifically we find that coupling exposures of  $\text{WF}_6$  with  $\text{Sn}(\text{acac})_2$  or  $\text{BCl}_3$  in a stepwise sequence acts to volatilize the  $\text{WO}_x\text{F}_y$  surface layer formed during  $\text{WF}_6$  etching, enabling etching of a fraction of a monolayer of  $\text{TiO}_2$  (i.e.,  $\sim 0.6$  Å) per ALE cycle at 170 °C.

## 2. EXPERIMENTAL SECTION

**a. List of Supplies and Materials.** The 99.99% tungsten hexafluoride ( $\text{WF}_6$ ) and 99.9% boron trichloride ( $\text{BCl}_3$ ) were purchased in stainless steel lecture bottles from Galaxy Chemical and Matheson, respectively. Trimethylaluminum (TMA) and titanium tetrachloride ( $\text{TiCl}_4$ ) were obtained from Strem Chemicals Inc. and used without further treatment. 99.9% tin acetylacetone ( $\text{Sn}(\text{acac})_2$ ) was purchased from Sigma-Aldrich. The Si substrates were boron doped Si(100) 6–10 Ω·cm (WRS Materials) and were used as-received. For the carrier and purge gas, dry 99.999% argon (Ar) was passed through an Entegris GateKeeper inert gas purifier to remove any residual water before entering the reactor.

**b. Reactor Design and Reaction Sequence.** Depositions were carried out in two home-built tubular hot-wall isothermal ALD reactors described in previous publications.<sup>35,36</sup> The chambers were heated resistively using PID controllers. The reaction chamber for the chemical vapor etching (CVE) experiments was ~60 cm long with a diameter of ~10 cm. The reactor for atomic layer etching (ALE) was a similar design with the same reactor length but with a smaller diameter of ~4 cm. Silicon substrates were loaded into the reactors and allowed to reach thermal equilibrium with the walls by flowing carrier gas for 30 min prior to deposition or etching.

In the larger CVE chamber, the baseline operating pressure was maintained at 1.5 Torr with an Ar carrier flow rate of 210 standard cubic centimeters per minute (sccm). The  $\text{WF}_6$  flow was restricted with a needle valve to generate a pressure increase of 300 mTorr over the baseline 1.5 Torr. The pulse sequence was  $\text{WF}_6/\text{Ar} = 1/60$  s, respectively. In some instances,  $\text{Sn}(\text{acac})_2$  was used in a  $\text{WF}_6/\text{Ar}/\text{Sn}(\text{acac})_2/\text{Ar}$  (1/60/1/60 s) sequence to increase the  $\text{WF}_6$  CVE etch rate.  $\text{Sn}(\text{acac})_2$  was heated to 105 °C to produce a pressure change of ~75 mTorr during dosing. Immediately prior to etching experiments,  $\text{Al}_2\text{O}_3$  and  $\text{TiO}_2$  ALD films were deposited in the same reaction chamber using an  $x/\text{Ar}/\text{H}_2\text{O}/\text{Ar}$  sequence where  $x$  is TMA and  $\text{TiCl}_4$  respectively, with a timing sequence of 0.25/45/0.25/45 s. In some cases, fresh ALD films were loaded into the reactor before etching. The data presented here were generally collected after preparing the surface with ALD metal oxide.

In the smaller ALE reactor, a  $\text{N}_2$  carrier flow rate of 150 sccm produced a baseline pressure of 800 mTorr. For the ALE runs, the typical reaction sequence followed  $\text{WF}_6/\text{N}_2/\text{BCl}_3/\text{N}_2 = 0.2/45/1/45$  s. During  $\text{WF}_6$  and  $\text{BCl}_3$  dosing, the pressure increase was approximately 600 and 800 mTorr, respectively. Under typical etch conditions, the short  $\text{WF}_6$  dose time in the ALE reactor produced a smaller net  $\text{WF}_6$  exposure per cycle compared to that during typical CVE. Prior to ALE,  $\text{Al}_2\text{O}_3$  and  $\text{TiO}_2$  ALD films were deposited using  $x/\text{Ar}/\text{H}_2\text{O}/\text{Ar}$  of 0.1/45/0.1/45 s, where  $x$  is either TMA or  $\text{TiCl}_4$ , respectively. The growth rate for the  $\text{TiO}_2$  ALD film was ~0.3 Å/cycle at 170 °C. The  $\text{WF}_6/\text{BCl}_3$  etching experiments were generally performed after preparing the reactor surface with ALD metal oxide.

**c. Sample Characterization.** Film deposition and etching were characterized using ex situ and in situ analytical tools. Spectroscopic ellipsometry (SE) data were obtained with a J.A. Woollam alpha-SE ellipsometer at an incidence angle of 70°. Chemical analysis was done using a SPECS X-ray photoelectron spectroscopy (XPS) system with a PHOIBOS 150 analyzer. Spectra were generated using an  $\text{Al K}\alpha$  X-ray source operated at 400 W. For all analyses, data reduction and fitting was carried out using CasaXPS software with charge compensation based on the C 1s (C–C, C–H) peak set to 285 eV. For some

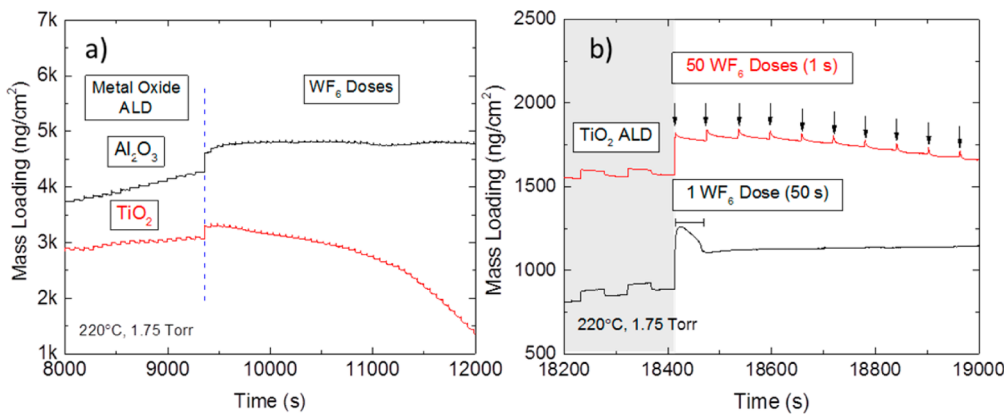


**Figure 1.** QCM analysis at 220 °C of (a) 200 cycles of  $\text{Al}_2\text{O}_3$  or  $\text{TiO}_2$  followed immediately by 50  $\text{WF}_6$ /Ar exposures of 1/60 s each and (b) initial loading of 1  $\text{WF}_6$  exposure of 50 s versus 50  $\text{WF}_6$ /Ar exposures of 1/60 s on  $\text{TiO}_2$  (200 cycles).

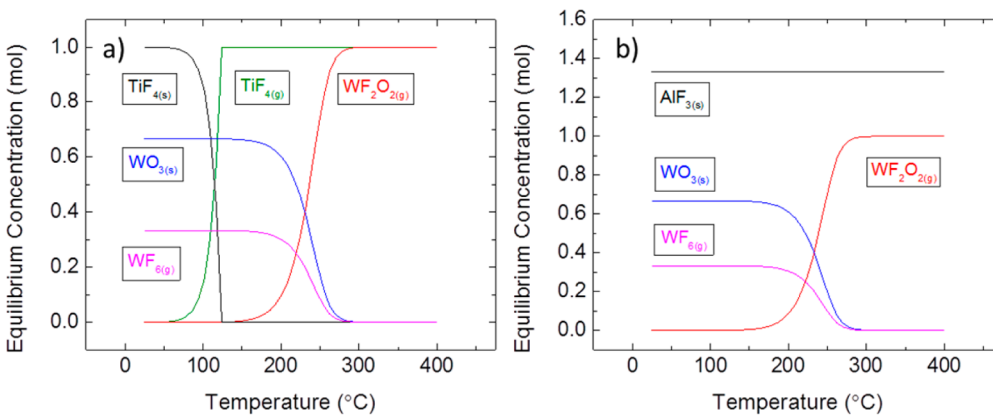


**Figure 2.** Thermodynamic modeling results showing the expected equilibrium species concentrations from 25 to 400 °C for  $\text{N}_2$ -diluted  $\text{WF}_6$  exposed to  $\text{TiO}_2$  or  $\text{Al}_2\text{O}_3$  at  $P = 1.5$  Torr: (a) 1 mol  $\text{WF}_6$  + 1 mol  $\text{TiO}_2$  and (b) 1 mol  $\text{WF}_6$  + 0.667 mol  $\text{Al}_2\text{O}_3$ .

analyses, we utilized the  $\text{Ti} 2p_{3/2}$  XPS peak intensity to estimate the thickness of  $\text{WO}_x\text{F}_y$  films formed as a result of  $\text{WF}_6$  adsorption. For this analysis, we measured the attenuation of the  $\text{Ti} 2p_{3/2}$  peak and modeled the film thickness using parameters available from the NIST Effective Attenuation Length Database,<sup>37</sup> coupled with electron inelastic mean-free path values determined using the TPP-2 M equation.<sup>38</sup> For this equation, we used a bandgap of 3.45 eV<sup>39</sup> and density of 3.58 g/cm<sup>3</sup>,<sup>40</sup> consistent with reported values for amorphous low density  $\text{WO}_3$  films.

Process conditions were further characterized using in situ QCM analysis. For these tests, a 6 MHz gold coated QCM crystal sensor (Inficon) was placed into the QCM housing. The crystal backside was purged with 45 sccm of Ar to prevent deposition on the back of the QCM crystal. Inclusion of a crystal back purge increased the operating pressure from 1.5 to 1.75 Torr. In the smaller ALE chamber, the QCM crystal backside was purged with 35 sccm of  $\text{N}_2$ , increasing the baseline pressure from 0.8 to 1 Torr. The mass change signals were detected by an Inficon SQM-160 monitor and recorded using a home designed LabVIEW program. The mass change reported from the QCM data provides reliable measurements of relative mass change under different process conditions. The measured frequency shifts are not specifically calibrated for quantitative analysis of individual mass change values.

**d. Thermodynamic Modeling.** Gibbs free energy values and equilibrium amounts in closed systems were calculated using HSC Chemistry 7.1 software. For the equilibrium composition calculations for the  $\text{WF}_6$  reaction, the starting input amounts were 5 mol of  $\text{N}_2$ , 1 mol of  $\text{WF}_6$ , and 1 mol of oxide ( $\text{TiO}_2$ ,  $\text{HfO}_2$ ,  $\text{ZrO}_2$ ,  $\text{SiO}_2$ , and  $\text{ZnO}$ ). The initial moles of  $\text{Al}_2\text{O}_3$  were set as 0.667 to compensate for reaction stoichiometry. For modeling the  $\text{BCl}_3$  reaction with the  $\text{WF}_6$  modified surface, the starting concentrations were 5 mol of  $\text{N}_2$ , 1 mol of metal fluoride ( $\text{TiF}_4$ ,  $\text{AlF}_3$ ,  $\text{ZrF}_4$ , etc.), 1 mol of  $\text{WO}_3$ , and 3 mol of

$\text{BCl}_3$ . For each data set, 50 calculations were done from 25 to 400 °C at 1.5 Torr (0.002 bar).

### 3. RESULTS AND DISCUSSION

#### Selective Chemical Vapor Etching of $\text{TiO}_2$ Using $\text{WF}_6$

The  $\text{WF}_6$  interaction with ALD metal oxide films at 220 °C was assessed with in situ QCM analysis, where the layer to be etched (either  $\text{Al}_2\text{O}_3$  or  $\text{TiO}_2$ ) is deposited in the reactor on the QCM crystal via ALD immediately before etching experiments. Deposition and etching were performed in the same reactor at the same temperature, without air exposure between ALD and etching. Figure 1a shows that immediately following steady-state  $\text{Al}_2\text{O}_3$  or  $\text{TiO}_2$  ALD at 220 °C, the first 3–5  $\text{WF}_6$  dose steps result in an increase in the mass loading of 355 and 226 ng/cm<sup>2</sup> for  $\text{Al}_2\text{O}_3$  and  $\text{TiO}_2$ , respectively. Additional  $\text{WF}_6$  exposures on the  $\text{Al}_2\text{O}_3$  surface lead to saturation, whereas additional  $\text{WF}_6$  exposures on the  $\text{TiO}_2$  surface lead to mass loss. After ~17  $\text{WF}_6$  doses, the QCM begins to record a net overall mass loss, and further  $\text{WF}_6$  dosing leads to additional mass loss, consistent with  $\text{TiO}_2$  etching by the  $\text{WF}_6$ . We note that the etch rate appears to increase as etching proceeds. For example, after 10  $\text{WF}_6$  doses, the etch rate is ~15 ng/cm<sup>2</sup> per  $\text{WF}_6$  dose but increases to ~87 ng/cm<sup>2</sup> per  $\text{WF}_6$  dose at 25  $\text{WF}_6$  doses. The increase in etch rate is attributed to the etch process transitioning through an incubation period before attaining steady state. This gives rise to an apparent thickness dependence in the etch rate, as discussed in detail in a further section below.

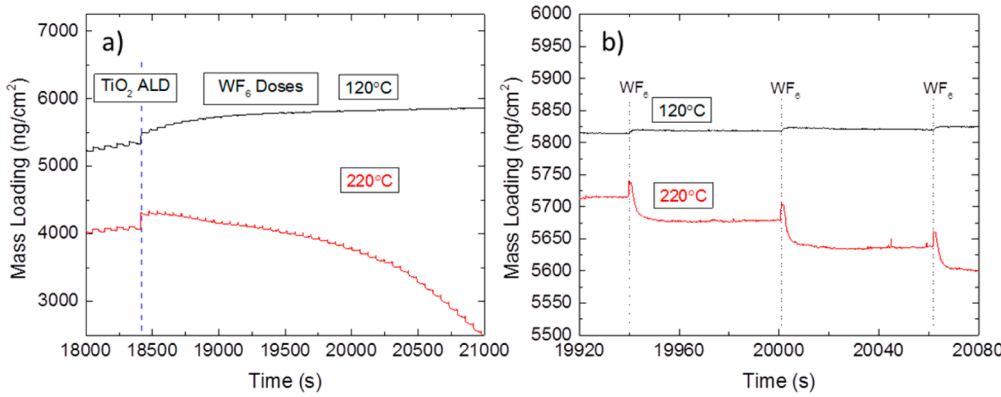


**Figure 3.** (a) QCM analysis of TiO<sub>2</sub> ALD followed by 50 WF<sub>6</sub> doses at 120 and 220 °C and (b) an enlarged view of the mass loading during the WF<sub>6</sub> doses, showing net mass loss during each WF<sub>6</sub> step at 220 °C and little to no change at 120 °C.

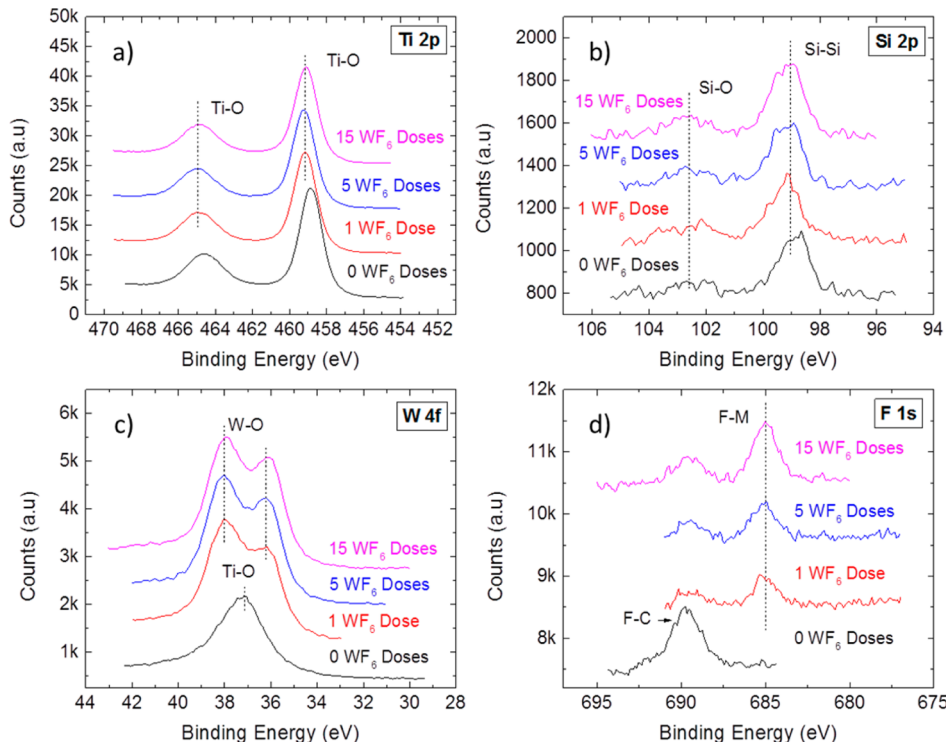


**Figure 4.** High resolution XPS scans of (a) Ti 2p, (b) Si 2p, (c) W 4f, and (d) F 1s regions for ~6.5 nm TiO<sub>2</sub> films exposed to 0, 1, 5, and 15 WF<sub>6</sub> doses at 220 °C.

Results in Figure 1b compare QCM mass response for a series of WF<sub>6</sub>/Ar = 1/60 s doses (as used in Figure 1a) with that for a single longer (50 s) WF<sub>6</sub> dose step. In these experiments, the Ar carrier flow rate was maintained at 210 sccm with a QCM back purge of 45 sccm for a baseline pressure of 1.75 Torr. The 50 s WF<sub>6</sub> dose increased the pressure by 250 mTorr. This pressure change and dose time corresponds approximately to a net exposure that is equivalent to 50 WF<sub>6</sub>/Ar pulses of 1/60 s each. The 50 s WF<sub>6</sub> pulse initially leads to a 360 ng/cm<sup>2</sup> mass increase, somewhat larger than for the individual dose steps (226 ng/cm<sup>2</sup>). As the WF<sub>6</sub> dose continued, the measured mass decreased, but after 50 s, QCM analysis shows a net mass increase of 205 ng/cm<sup>2</sup> relative to the mass measured immediately following TiO<sub>2</sub> ALD. On the basis of data and modeling presented below, the initial mass increase during the WF<sub>6</sub> dosing period is ascribed to fluorine and tungsten uptake on the TiO<sub>2</sub> surface, and the mass

decrease during further exposure corresponds to etching via desorption of TiF<sub>4</sub> and WF<sub>2</sub>O<sub>2</sub> vapor products. In this case, the 50 WF<sub>6</sub>/Ar pulses of 1/60 s leads to more etching than a single 50 s WF<sub>6</sub> pulse because the purge provided time to promote etch product volatilization.

**Thermodynamic Modeling of Metal Oxide Chemical Vapor Etching by WF<sub>6</sub>.** Thermodynamic calculations based on minimizing free energy were performed to determine probable product species and to shed light on expected differences for etching of Al<sub>2</sub>O<sub>3</sub> and TiO<sub>2</sub> by WF<sub>6</sub>. The (unbalanced) overall reaction follows:

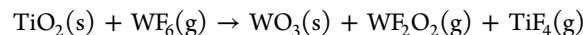
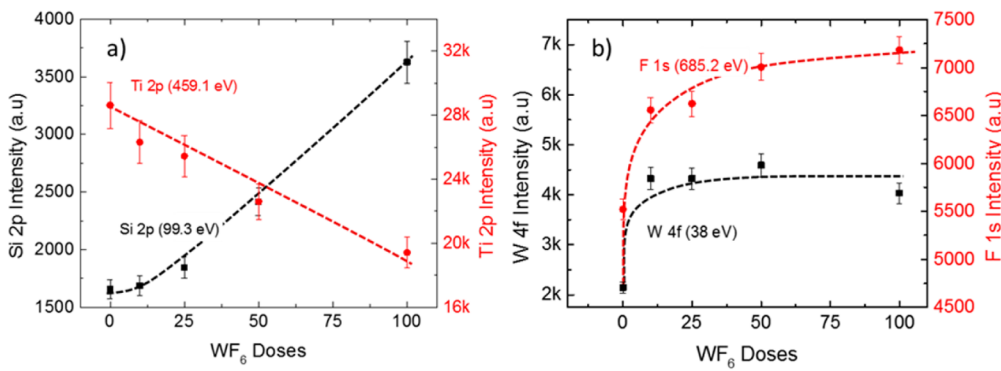
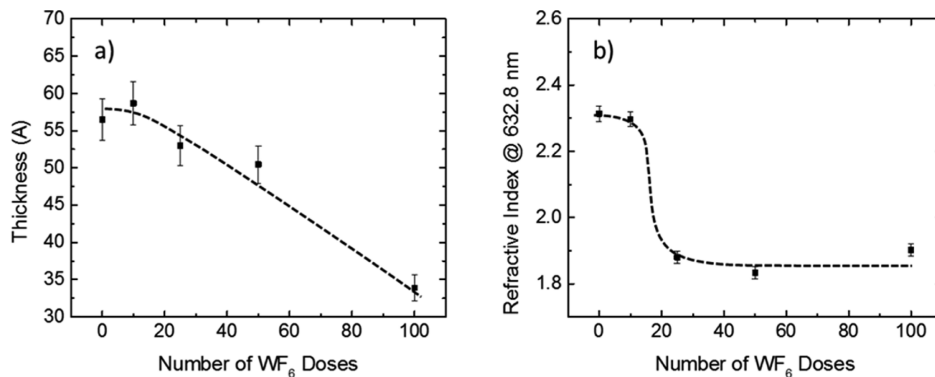


Figure 2a shows the calculated equilibrium composition for a closed system initially consisting of 1:1 molar ratio of TiO<sub>2</sub> to WF<sub>6</sub> as temperatures changes from 25 to 400 °C. At room temperature WF<sub>6</sub> reacts with TiO<sub>2</sub> to form solid WO<sub>3</sub> and solid



**Figure 5.** Peak intensity of high resolution XPS scans of (a) Ti 2p (459.1 eV) and Si 2p (99.3 eV) and (b) W 4f and (38 eV) and F 1s (685.2 eV) for 5.5 nm TiO<sub>2</sub> films exposed to 0, 10, 25, 50, and 100 WF<sub>6</sub> doses at 220 °C. Lines are a guide for the eye. The decrease in the Ti 2p signal confirms film etching.



**Figure 6.** (a) Thickness and (b) refractive index at 632.8 nm of samples with 5.5 nm TiO<sub>2</sub> followed by 0, 15, 25, 50, and 100 WF<sub>6</sub> doses at 220 °C, measured with spectroscopic ellipsometry. Lines are a guide to the eye.

TiF<sub>4</sub>, and at ~125 °C the solid TiF<sub>4</sub> completely volatilizes. At ~150 °C, WF<sub>6</sub> begins to etch the solid WO<sub>3</sub> to form volatile WF<sub>2</sub>O<sub>2</sub>. Similar modeling also indicates that WF<sub>6</sub> will etch SiO<sub>2</sub>, though SiO<sub>2</sub> differs from TiO<sub>2</sub> because, unlike TiF<sub>4</sub>, SiF<sub>4</sub> is volatile even at room temperature. It should be noted that, in the calculations, when either the initial WF<sub>6</sub>:oxide ratio or the Ar partial pressure is increased, the temperature required to generate the volatile products decreases, indicating more favorable etching. This analysis is strictly accurate only for closed systems, where products are not purged.

Similar modeling results for Al<sub>2</sub>O<sub>3</sub> shown in Figure 2b suggest that WF<sub>6</sub> reacts at room temperature with Al<sub>2</sub>O<sub>3</sub> to form solid WO<sub>3</sub> and solid AlF<sub>3</sub>. At higher temperatures, like the case of TiO<sub>2</sub>, the solid WO<sub>3</sub> reacts further with WF<sub>6</sub> to form volatile WF<sub>2</sub>O<sub>2</sub>. However, the AlF<sub>3</sub> remains nonvolatile up to 400 °C. This solid AlF<sub>3</sub> layer likely passivates the surface, preventing etching.<sup>21,22,41</sup> Similar models for ZnO, ZrO<sub>2</sub>, and HfO<sub>2</sub> showed favorable free energy changes for fluorination by WF<sub>6</sub> forming nonvolatile metal fluorides. This shows that favorable etching reactions require both favorable surface reactions as well as volatile product formation.

**Process Temperature and WF<sub>6</sub> Chemical Vapor Etching Behavior.** The etching behavior of TiO<sub>2</sub> by WF<sub>6</sub> was assessed experimentally at different temperatures to collaborate the thermodynamic analysis. Data from QCM analysis in Figure 3a shows that when the temperature was reduced from 220 to 120 °C, the initial 1–5 WF<sub>6</sub> doses result in a mass gain on the TiO<sub>2</sub> surface. Additional WF<sub>6</sub> doses are accompanied by relatively small mass increases, which plateau with time. The enlarged view in Figure 3b further shows the

response to the WF<sub>6</sub> doses at 220 and 120 °C, in which there are clear mass losses following the WF<sub>6</sub> doses at 220 °C.

**Analysis of WF<sub>6</sub> Chemical Vapour Etching of TiO<sub>2</sub> by XPS and Ellipsometry.** The composition of the TiO<sub>2</sub> surfaces following the initial few WF<sub>6</sub> cycles, i.e., prior to significant TiO<sub>2</sub> mass loss, was analyzed with ex situ XPS analysis. Figure 4 shows high resolution XPS scans of TiO<sub>2</sub> surfaces after 0, 1, 5, and 15 WF<sub>6</sub> doses. For this analysis, the initial TiO<sub>2</sub> film was sufficiently thin (i.e., ~6.5 nm) to allow detection of the underlying Si substrate. In addition, the starting TiO<sub>2</sub> shows evidence for fluorine at ~690 eV, consistent with fluoride from the reactor, likely remaining from previous WF<sub>6</sub> etch experiments. Figure 4a shows the Ti 2p signal decreases slightly following 1, 5, and 15 WF<sub>6</sub> doses, but the Si 2p signal intensity in Figure 4b stays relatively constant. The presence of surface tungsten and fluorides is confirmed by results in Figure 4c,d, showing W 4f and F 1s peaks on the TiO<sub>2</sub> surface after 1 WF<sub>6</sub> dose. The tungsten signal stays relatively constant between 1 and 15 WF<sub>6</sub> doses, whereas the F 1s peak at 685 eV (associated with metal fluorides) progressively increases. This is consistent with WF<sub>6</sub> fluorinating the TiO<sub>2</sub> surface and with fluorine diffusion into the TiO<sub>2</sub> subsurface.<sup>42,43</sup>

The relative location of the XPS peaks provides additional information concerning the etching mechanisms. For example, after 15 WF<sub>6</sub> doses, the Ti 2p doublet shifts by ~0.4 eV to higher binding energy (i.e., the Ti 2p<sub>3/2</sub> peak shifts from 459.2 to 458.8 eV). This increase in binding energy is consistent with highly electronegative surface species on the TiO<sub>2</sub> such as WO<sub>x</sub>F<sub>y</sub> or TiO<sub>y</sub>F<sub>y</sub>. Full titanium fluorination to TiF<sub>3</sub> or TiF<sub>4</sub> would produce a much larger shift in the Ti 2p<sub>3/2</sub> peaks to 462

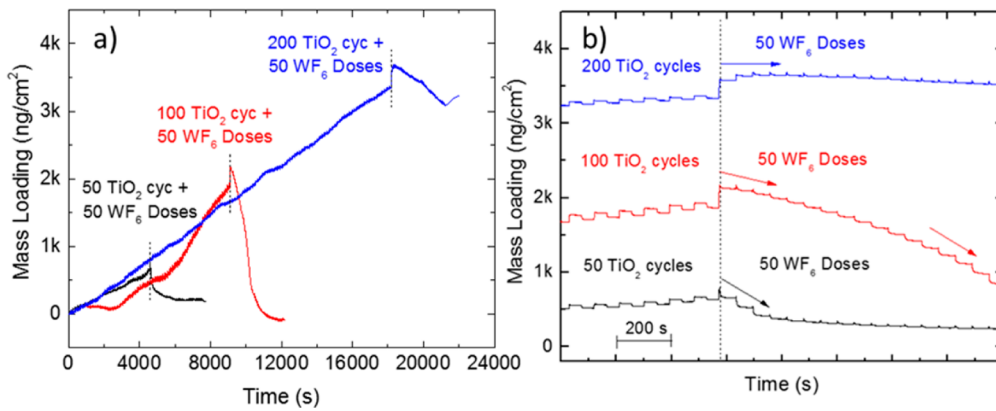


**Figure 7.** (a) QCM analysis of WF<sub>6</sub> etching following 50, 100, and 200 TiO<sub>2</sub> ALD cycles on a bare Au QCM crystal at 220 °C and 1.75 Torr. (b) Enlarged view of WF<sub>6</sub> etching showing an “incubation” period for the vapor etching that is dependent on the initial TiO<sub>2</sub> film thickness.

and 464 eV, respectively.<sup>43</sup> In addition, the W 4f doublet peaks at 37.9 and 36 eV are shifted ~0.5 eV to higher binding energy compared to oxidized tungsten (37.6 and 35.5 eV),<sup>35,44</sup> again consistent with surface fluorides.<sup>45</sup>

Figure 5a shows the Ti 2p and Si 2p peak intensity values collected from the high resolution XPS scans plotted versus number of WF<sub>6</sub> dose steps (i.e., WF<sub>6</sub> exposure) after 0, 15, 25, 50, and 100 WF<sub>6</sub> doses. More WF<sub>6</sub> exposures lead to a linear decrease in the Ti signal and an increase in signal from the silicon substrate, as expected for etching of TiO<sub>2</sub>. Some initial decrease in the Ti 2p signal is ascribed to surface tungsten oxide. The W 4f signal associated with oxidized tungsten (Figure 5b) increases rapidly and stays constant, even up to 100 WF<sub>6</sub> doses. Figure 5b also shows that the F 1s signal increases significantly within the first 10 WF<sub>6</sub> doses followed by saturating behavior with additional WF<sub>6</sub> exposure.

The film thickness for the samples in Figure 5 was further analyzed by spectroscopic ellipsometry, and results are shown in Figure 6. Figure 6a shows that, for the first few WF<sub>6</sub> cycles, the physical film thickness slightly increases, consistent with formation of a tungsten oxy-fluoride surface layer. As WF<sub>6</sub> dosing proceeds, the TiO<sub>2</sub> film thickness decreases, consistent with etching observed by QCM and XPS in Figures 1, 3, and 5. Furthermore, the refractive index at 632.8 nm for the TiO<sub>2</sub> films is ~2.3 after 0 and 10 WF<sub>6</sub> doses but decreases to ~1.9 with 25–100 WF<sub>6</sub> doses. The decrease in refractive index can be correlated with a decrease in film density. The observed decrease suggests that the WF<sub>6</sub> exposure promotes formation of a porous WO<sub>3</sub> film<sup>40,46</sup> or the formation of a low density WO<sub>x</sub>F<sub>y</sub> surface layer.<sup>32,33</sup>

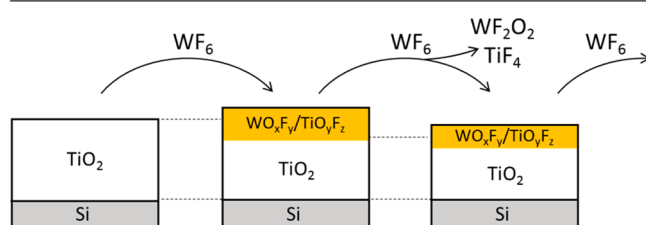
**Incubation of Chemical Vapor Etching and Effect of TiO<sub>2</sub> Film Thickness.** The results in Figure 1a suggest that the etch rate increases as the etching proceeds. We hypothesized, therefore, that the WF<sub>6</sub> etch rate may depend on the thickness of the initial TiO<sub>2</sub> layer. We tested this by monitoring QCM crystals coated with 50, 100, and 200 cycles of ALD TiO<sub>2</sub> at 220 °C (estimated to be 10, 25, 55 Å thick), each followed by 50 WF<sub>6</sub>/Ar dose steps. Results are given in Figure 7. In this data set, the trace for 200 TiO<sub>2</sub> ALD cycles + 50 WF<sub>6</sub> doses is reproduced from Figures 1 and 3. Note that these experiments required continuous data collection over 3–5 h, and in Figure 7a, the long-period fluctuations in the QCM data result from small instabilities in the controlled reactor temperature.

Figure 7b reproduces the results from Figure 7a on an expanded time scale, shifted to align the first WF<sub>6</sub> dose step.

Note that the mass loading scale on the y-axis remains the same as in Figure 7a, allowing the relative rates of mass loss to be directly compared. Figure 7b clearly shows that, during the initial WF<sub>6</sub> doses, the rate of mass loss is slow for the thickest (200 cycle) TiO<sub>2</sub> film and relatively fast for the thin (50 cycle) ALD TiO<sub>2</sub>. For the 200 cycle TiO<sub>2</sub> layer, after an initial mass gain of ~250 ng/cm<sup>2</sup>, the first 25 etch cycles produce no mass loss, after which etching readily proceeds (as shown in Figure 7a), indicating etch “incubation”. For the 100 cycle TiO<sub>2</sub> film, the first WF<sub>6</sub> dose also produces mass gain, and etching proceeds with less incubation time, attaining steady-state etching after several WF<sub>6</sub>/Ar doses. For the thinnest (50 cycle) TiO<sub>2</sub> film, the mass gain is only 28 ng/cm<sup>2</sup> during the initial WF<sub>6</sub> dose, and relatively fast etching proceeds after the first dose, slowing after ~5 WF<sub>6</sub>/Ar doses, consistent with complete TiO<sub>2</sub> removal.

The apparent higher etch rate for the thinnest starting TiO<sub>2</sub> layer is ascribed, therefore, to a shorter incubation period for the thinner films to reach steady-state etching. This etch incubation arises because a thin starting film requires fewer WF<sub>6</sub> doses to attain the surface fluorine concentration required to volatilize surface products. A thicker starting film can draw more fluorine into the film bulk, thereby needing more WF<sub>6</sub> doses before etching begins.

**Schematic of the WF<sub>6</sub> Chemical Vapor Etch Reaction Process.** Figure 8 shows the proposed WF<sub>6</sub> chemical vapor etching mechanism of TiO<sub>2</sub> films at 220 °C based on QCM, XPS, and ellipsometry analysis. First, during the initial WF<sub>6</sub> doses, WF<sub>6</sub> adsorbs and reacts with the TiO<sub>2</sub> surface, forming a low density WO<sub>x</sub>F<sub>y</sub>/TiO<sub>y</sub>F<sub>z</sub> layer. Analysis of the XPS results confirms mixing of metal oxides in this layer. If the top layer



**Figure 8.** Schematic of the chemical vapor etching mechanism for TiO<sub>2</sub> films exposed to WF<sub>6</sub> at 220 °C: (1) WF<sub>6</sub> adsorbs on thick TiO<sub>2</sub> surface, forming surface-bound TiO<sub>y</sub>F<sub>z</sub> and WO<sub>x</sub>F<sub>y</sub>, (2) Additional WF<sub>6</sub> exposure further fluorinates the TiO<sub>y</sub>F<sub>z</sub> and WO<sub>x</sub>F<sub>y</sub>, creating volatile WF<sub>2</sub>O<sub>2</sub> and TiF<sub>4</sub>, etching the TiO<sub>2</sub> film.

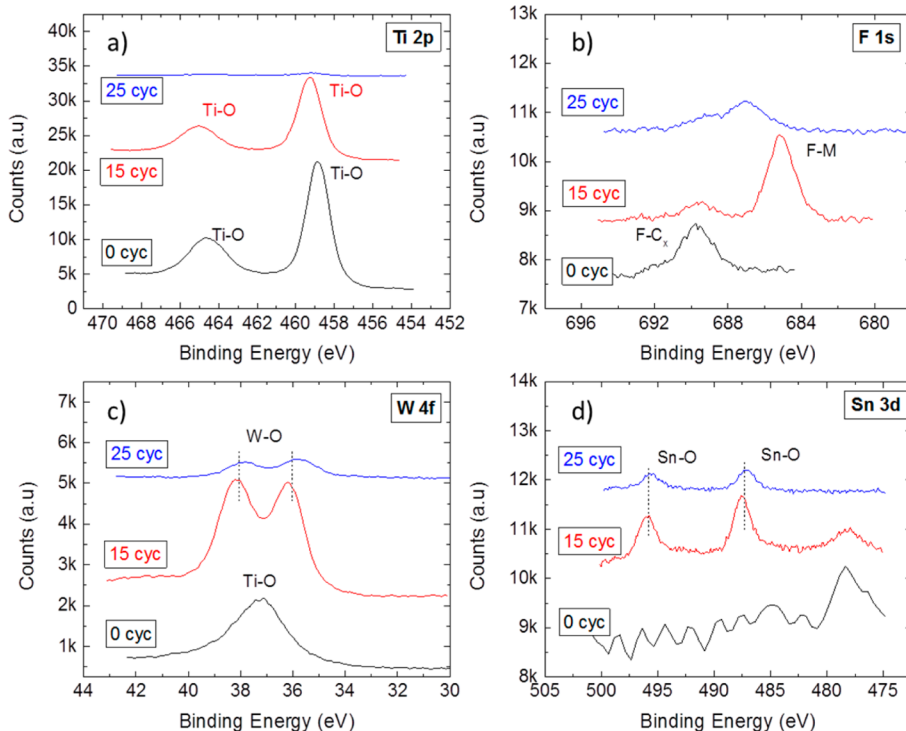


**Figure 9.** High resolution XPS scans of (a) Ti 2p, (b) F 1s, (c) W 4f, and (d) Sn 3d regions for 6.5 nm TiO<sub>2</sub> films following 0, 15, and 25 WF<sub>6</sub>/Ar/Sn(acac)<sub>2</sub>/Ar cycles at 220 °C and 1.75 Torr.

consisted of only WO<sub>x</sub>F<sub>y</sub>, then (using a density of  $\sim$ 3.6 g/cm<sup>3</sup> reported<sup>40</sup> for low density WO<sub>3</sub>) a mass increase of  $\sim$ 250 nm/cm<sup>2</sup> during the first WF<sub>6</sub> dose (shown in Figure 1 at 220 °C) would correspond to a WO<sub>x</sub>F<sub>y</sub> layer that is  $\sim$ 4–6 Å thick. However, after 1 WF<sub>6</sub> exposure, the attenuation of the Ti 2p<sub>3/2</sub> XPS signal is about 2–3 times less than expected for an  $\sim$ 6 Å WO<sub>x</sub>F<sub>y</sub> layer, consistent with the presence of nonvolatile TiF<sub>3</sub><sup>42,46</sup> and TiOF<sub>2</sub><sup>47</sup> with WO<sub>3</sub>.<sup>32,33,46,48</sup>

During the initial WF<sub>6</sub>, the observed net mass gain for thick starting TiO<sub>2</sub> indicates that the extent of surface fluorination within the mixed WO<sub>x</sub>F<sub>y</sub>/TiO<sub>y</sub>F<sub>z</sub> surface layer is not sufficient to produce a significant amount of volatile products. Subsequent WF<sub>6</sub> doses further fluorinate the surface-bound WO<sub>x</sub>F<sub>y</sub> and TiO<sub>y</sub>F<sub>z</sub> producing volatile etch products, including WO<sub>2</sub>F<sub>2</sub> and TiF<sub>4</sub>, as indicated by the equilibrium thermodynamics results in Figure 2. Some surface fluorine will diffuse and remain within the underlying oxide.<sup>42,43,49,50</sup> A relatively thick starting TiO<sub>2</sub> layer provides a large “sink” for fluorine diffusion, whereas a thin TiO<sub>2</sub> layer allows rapid surface fluorination. This results in a thickness-dependent incubation time for the onset of etching, displayed in the QCM results in Figure 7. We also note that, during the purge step at steady state, volatilization of metal fluorides and metal oxy-fluorides reduces the fluoride concentration in the surface layer. Etching stops when the surface fluoride density is not sufficient to support further vaporization. This is supported by the QCM results in Figures 1, 3, and 7 where the mass loading reaches a steady plateau during the WF<sub>6</sub> purge step. This mechanism for etching is consistent with results from Kobayashi et al.<sup>32</sup> showing that WF<sub>6</sub> reacts with SiO<sub>2</sub> to form volatile WOF<sub>4</sub> and SiF<sub>4</sub>. Furthermore, in similar systems, WF<sub>6</sub> has been shown to etch WO<sub>3</sub> films<sup>33</sup> and NbCl<sub>5</sub> was observed to etch Nb<sub>2</sub>O<sub>5</sub> films by forming volatile NbOCl<sub>3</sub>.<sup>34</sup>

#### Co-Reagents To Modify TiO<sub>2</sub> Chemical Vapor Etching.

On the basis of the XPS analysis in Figures 4 and 5, the TiO<sub>2</sub> chemical vapor etching by WF<sub>6</sub> produces a thin layer of WO<sub>x</sub>F<sub>y</sub> on the etched TiO<sub>2</sub> surface. To explore approaches to avoid or remove this layer, we performed several experiments. As one approach, Sn(acac)<sub>2</sub> was incorporated into the CVE sequence at 220 °C. Sn(acac)<sub>2</sub> has been observed to assist in metal fluoride volatilization in similar atomic layer etching processes.<sup>20–22,24</sup> For this experiment, we deposited 200 cycles of TiO<sub>2</sub> at 220 °C, and then etched at the same temperature using a WF<sub>6</sub>/Ar/Sn(acac)<sub>2</sub>/Ar sequence of 1/60/1/60 s. Figure 9 shows high resolution XPS scans collected after 6.5 nm of TiO<sub>2</sub> ALD (0 etch cycles) and after TiO<sub>2</sub> ALD followed by 15 and 25 WF<sub>6</sub>/Sn(acac)<sub>2</sub> etch cycles. We first note that at 220 °C, the WF<sub>6</sub>/Sn(acac)<sub>2</sub> sequence leads to loss of the Ti 2p signal, indicating film etching. Comparing the measured XPS intensities in Figure 9 to those in Figure 5 (with only WF<sub>6</sub> exposure steps), the addition of Sn(acac)<sub>2</sub> significantly increases the etch rate for an  $\sim$ 6.5 nm TiO<sub>2</sub> film, so that after 25 WF<sub>6</sub>/Sn(acac)<sub>2</sub> cycles the Ti 2p signal is near the detection limit ( $\sim$ 0.5 atom %). We also note the presence of surface tin after 15 and 25 cycles at 220 °C. After 25 WF<sub>6</sub>/Sn(acac)<sub>2</sub> cycles, the amount of surface fluorine and tungsten is less than observed in Figure 5 after 25 WF<sub>6</sub> cycles. These results suggest that the addition of Sn(acac)<sub>2</sub> into the WF<sub>6</sub>/Ar sequential etch process increases the etch rate by creating additional volatile etch products such as TiO(acac)<sub>2</sub> or TiF<sub>2</sub>(acac)<sub>2</sub>.<sup>20</sup>

#### Low Temperature TiO<sub>2</sub> Atomic Layer Etching Using

WF<sub>6</sub>/BCl<sub>3</sub>. As shown above in Figures 5 and 6, TiO<sub>2</sub> CVE at 220 °C proceeds nearly continuously without evidence for self-limiting behavior. A self-limiting atomic layer etching (ALE) process, consisting of self-limiting adsorption and activation steps, is more desirable in that it will allow the extent of etching

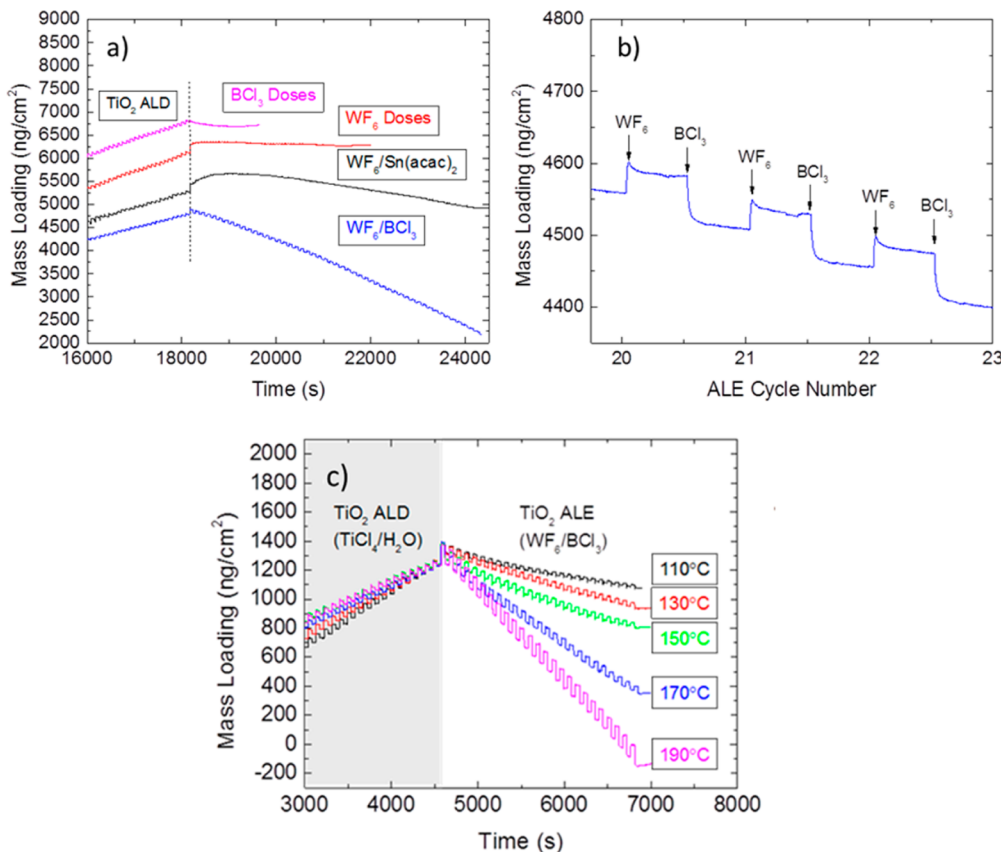


**Figure 10.** (a) QCM analysis at 170 °C and 1.75 Torr of TiO<sub>2</sub> ALD followed by 25 BCl<sub>3</sub>/Ar doses (pink), 50 WF<sub>6</sub>/Ar doses (red), 50 WF<sub>6</sub>/Ar/Sn(acac)<sub>2</sub>/Ar cycles (black), or 50 WF<sub>6</sub>/Ar/BCl<sub>3</sub>/Ar cycles (blue). (b) Enlarged view of the WF<sub>6</sub>/Ar/BCl<sub>3</sub>/Ar etch sequence. (c) QCM of WF<sub>6</sub>/Ar/BCl<sub>3</sub>/Ar sequence at 110, 130, 150, 170, and 190 °C.

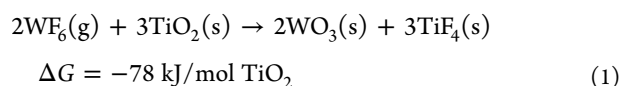
to be well controlled and defined. Therefore, we worked to modify the WF<sub>6</sub>/Ar/Sn(acac)<sub>2</sub>/Ar reaction sequence to identify possible ALE conditions. Using the results in Figures 2, 3, and 8, we (1) reduced the process temperature from 220 to 170 °C to prevent uncontrolled WF<sub>6</sub> etching and (2) explored BCl<sub>3</sub> as an alternative coreagent in place of Sn(acac)<sub>2</sub> to volatilize surface-adsorbed product species.

Figure 10a shows QCM results collected at 170 °C. For each run, TiO<sub>2</sub> ALD was performed for at least 100 cycles, followed immediately by exposure to (i) BCl<sub>3</sub>/Ar doses; (ii) WF<sub>6</sub>/Ar doses; (iii) WF<sub>6</sub>/Ar/Sn(acac)<sub>2</sub>/Ar cycles; or (iv) WF<sub>6</sub>/Ar/BCl<sub>3</sub>/Ar cycles. At 170 °C, without the additional coreagent, WF<sub>6</sub> shows initial mass gain consistent with surface adsorption, followed by a plateau indicating little to no TiO<sub>2</sub> etching. Dosing only BCl<sub>3</sub> appears to initially etch the TiO<sub>2</sub>, but like the WF<sub>6</sub>, additional BCl<sub>3</sub> does not lead to substantial etching. In contrast, the WF<sub>6</sub>/Sn(acac)<sub>2</sub> sequence produces an initialization period in which the mass increases, followed by controlled layer-by-layer etching.

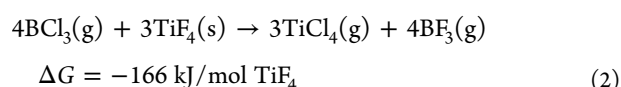
Figure 10a shows that the WF<sub>6</sub>/BCl<sub>3</sub> sequence yields stepwise linear etching, but unlike the WF<sub>6</sub>/Sn(acac)<sub>2</sub> sequence, it starts immediately from the first BCl<sub>3</sub> exposure step. An expanded view of the steady-state WF<sub>6</sub>/BCl<sub>3</sub> etching process is shown in Figure 10b. The mass gain during the WF<sub>6</sub> dose at steady state is ~29 ng/cm<sup>2</sup>. A larger mass uptake is observed during the first WF<sub>6</sub> dose. After one complete WF<sub>6</sub>/BCl<sub>3</sub> cycle, the mass change is ~53 ng/cm<sup>2</sup>/cycle, indicating an etch rate that is larger than the 26 ng/cm<sup>2</sup> per cycle mass gain measured during TiO<sub>2</sub> ALD at the same process temperature.

Figure 10c shows QCM results for process temperatures between 110 and 190 °C for WF<sub>6</sub>/Ar/BCl<sub>3</sub>/Ar = 0.2/45/1/45 s. The etch rate is nearly independent of temperature between ~110° and 150 °C, consistent with an “ALE temperature window” in this range. This range corresponds to limited volatility of TiF<sub>4</sub>,<sup>51,52</sup> suggesting that product elimination is a likely rate-limiting step for the ALE reaction mechanism. Higher temperature generally promotes fluorine diffusion during the WF<sub>6</sub> dose, and increases the rate of etch product volatilization, leading to an overall faster etch rate.

**Thermodynamic Modeling of WF<sub>6</sub>/BCl<sub>3</sub> ALE of TiO<sub>2</sub> and Al<sub>2</sub>O<sub>3</sub>.** Thermodynamic modeling of the WF<sub>6</sub>/BCl<sub>3</sub> ALE reaction was also performed. The expected etch stoichiometry and Gibbs free energy change at 170 °C are given. The first WF<sub>6</sub> dose leads to surface adsorption and fluorination:



The stoichiometric solid products, WO<sub>3</sub> and TiF<sub>4</sub>, are used in the ΔG analysis to represent the expected solid WO<sub>x</sub>F<sub>y</sub>/TiO<sub>v</sub>F<sub>z</sub> surface layer. At 170°C, TiF<sub>4</sub> vapor is also an expected product. The BCl<sub>3</sub> dose then allows ligand exchange that activates and volatilizes the solid reaction products:



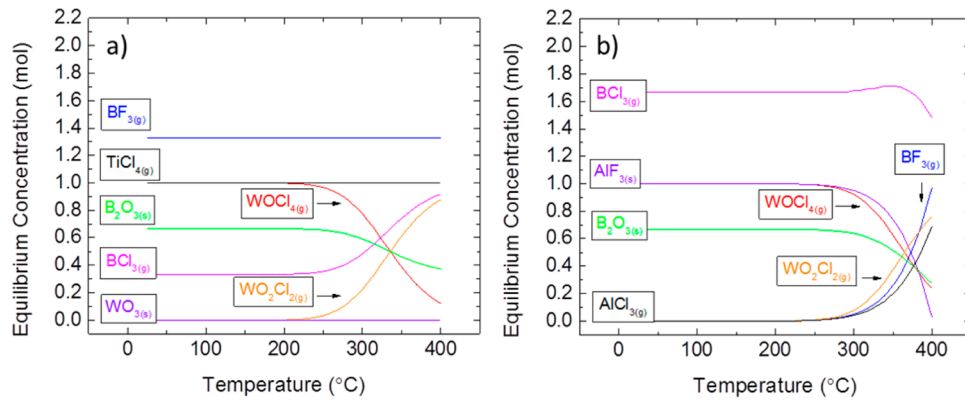


**Figure 11.** Thermodynamic modeling results showing the expected equilibrium species concentrations from 25 to 400 °C for (a) reactions 2 and 3, exposing N<sub>2</sub>-diluted BCl<sub>3</sub> at 1.5 Torr to TiF<sub>4</sub>/WO<sub>3</sub>; 3 mol of BCl<sub>3(g)</sub> + 1 mol of TiF<sub>4(s)</sub> + 1 mol of WO<sub>3(s)</sub>; and (b) the analogous reactions for the Al<sub>2</sub>O<sub>3</sub> system: 3 mol of BCl<sub>3(g)</sub> + 1 mol of AlF<sub>3(s)</sub> + 1 mol of WO<sub>3(s)</sub>. At equilibrium at 170 °C, BCl<sub>3</sub> + TiF<sub>4</sub>/WO<sub>3</sub> produces predominantly volatile BF<sub>3</sub>, TiCl<sub>4</sub>, and WOCl<sub>4</sub> and solid B<sub>2</sub>O<sub>3</sub>.

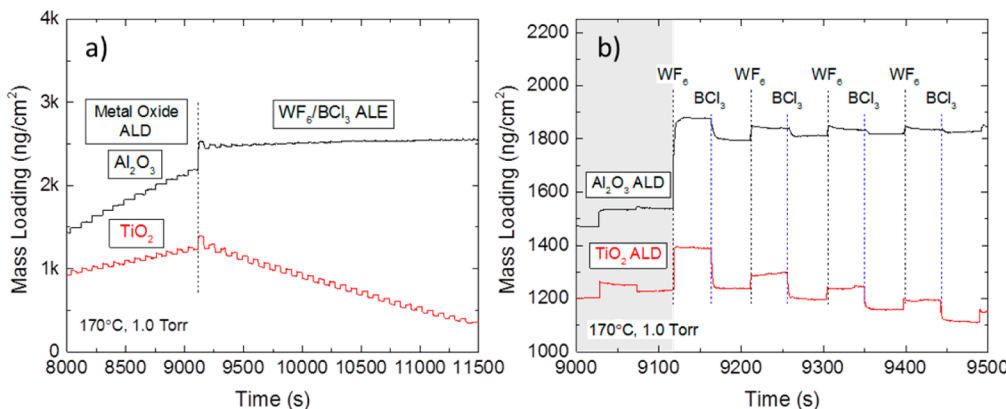
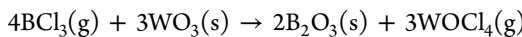
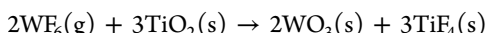


**Figure 12.** (a) QCM analysis of Al<sub>2</sub>O<sub>3</sub> and TiO<sub>2</sub> ALD followed by 50 WF<sub>6</sub>/BCl<sub>3</sub> ALE cycles at 170 °C. The ALE sequence follows WF<sub>6</sub>/Ar/BCl<sub>3</sub>/Ar (0.2/45/2.5/60 s). (b) Enlarged view of (a).

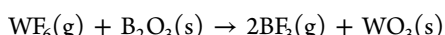


$$\Delta G = -83 \text{ kJ/mol WO}_3 \quad (3)$$

Some surface fluorine also remains as a TiF<sub>y</sub>O<sub>z</sub>(s) product.<sup>47</sup> Subsequent WF<sub>6</sub> doses repeat the TiO<sub>2</sub> surface adsorption and fluorination shown in (1) (repeated here as 4) and also activate and volatilize the surface boron oxide:



$$\Delta G = -78 \text{ kJ/mol TiO}_2 \quad (4)$$



$$\Delta G = -203 \text{ kJ/mol B}_2\text{O}_3 \quad (5)$$

The expected equilibrium thermodynamics for the WF<sub>6</sub> activation step (reaction 1 or reaction 4) was previously given in Figure 2. That figure also shows the case of WF<sub>6</sub> reaction with Al<sub>2</sub>O<sub>3</sub>. At 170 °C in Figure 2, the main surface species are solid WO<sub>3</sub> and metal fluorides, i.e., AlF<sub>3</sub> on Al<sub>2</sub>O<sub>3</sub>, and TiO<sub>y</sub>F<sub>z</sub> on TiO<sub>2</sub>. Figure 11 shows the thermodynamic results for the second half-reaction in the ALE sequence (e.g., reactions 2 and 3), when BCl<sub>3</sub> is exposed to solid WO<sub>3</sub> and metal fluoride (TiF<sub>4</sub> or AlF<sub>3</sub>). Figure 11a shows that, at low temperature, BCl<sub>3</sub> reacts with TiF<sub>4</sub> and WO<sub>3</sub> to form volatile TiCl<sub>4</sub>, WOCl<sub>4</sub>, and BF<sub>3</sub>, along with solid B<sub>2</sub>O<sub>3</sub>, consistent with the reaction stoichiometry in eqs 2 and 3. Similar modeling of

reaction 5 also shows consistent results. Although not included in the figure, the model suggests that at low temperatures a small amount of solid WO<sub>x</sub>Cl<sub>y</sub> species may also form via elimination of Cl<sub>2</sub>. Additionally, other modeling studies (not shown) indicate that the WF<sub>6</sub>/BCl<sub>3</sub> process is thermodynamically favorable for etching HfO<sub>2</sub> and ZrO<sub>2</sub>, but a somewhat higher process temperature is needed because HfCl<sub>4</sub> and ZrCl<sub>4</sub> are less volatile than TiCl<sub>4</sub>.

In contrast to the favorable etching of TiO<sub>2</sub> or other oxides with WF<sub>6</sub>/BCl<sub>3</sub>, modeling results in Figures 2b and 11b indicate that Al<sub>2</sub>O<sub>3</sub> etching is not thermodynamically favorable at low temperature. With Al<sub>2</sub>O<sub>3</sub>, Figure 2b shows that WF<sub>6</sub> will readily form tungsten oxides, and in Figure 11b, the BCl<sub>3</sub> will react with WO<sub>3</sub> to form volatile WOCl<sub>4</sub>. However, the solid AlF<sub>3</sub> remains stable up to ~300 °C where it then reacts to form the AlCl<sub>3</sub> vapor. Other modeling results indicate that low oxidation state metal oxides such as ZnO, CoO, and CuO are also not etched by WF<sub>6</sub>/BCl<sub>3</sub> until T > 350 °C because of the low volatility of the corresponding metal chloride. Overall, these results indicate that the WF<sub>6</sub>/BCl<sub>3</sub> etch sequence is overall thermodynamically favorable for etching TiO<sub>2</sub> at 170 °C but not favorable for etching Al<sub>2</sub>O<sub>3</sub> at the same process temperature. The data in the following section test this expectation experimentally.

#### Experimental Analysis of WF<sub>6</sub>/BCl<sub>3</sub> ALE Selectivity.

The selectivity of WF<sub>6</sub>/BCl<sub>3</sub> ALE for TiO<sub>2</sub> versus Al<sub>2</sub>O<sub>3</sub> was assessed with QCM at 170 °C, and results are given in Figure

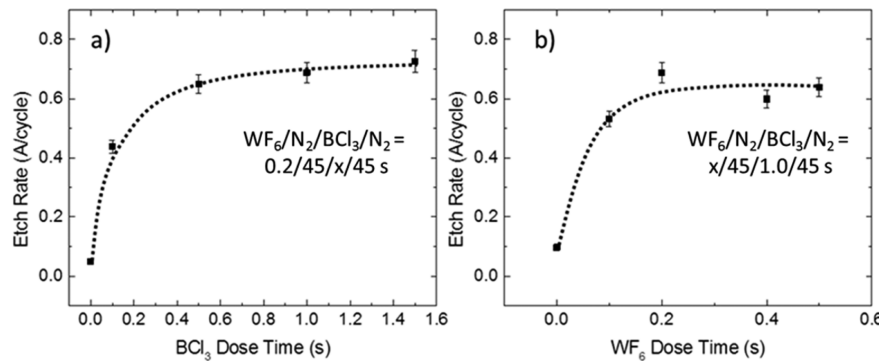


**Figure 13.** Etch rates at 170 °C for TiO<sub>2</sub>: (a) BCl<sub>3</sub> with a constant WF<sub>6</sub> dose time of 0.2 s and (b) WF<sub>6</sub> dose time with a constant BCl<sub>3</sub> exposure time of 1 s. The ALE reactor was conditioned with 200 TiO<sub>2</sub> ALD cycles after every 3 subsequent ALE runs.

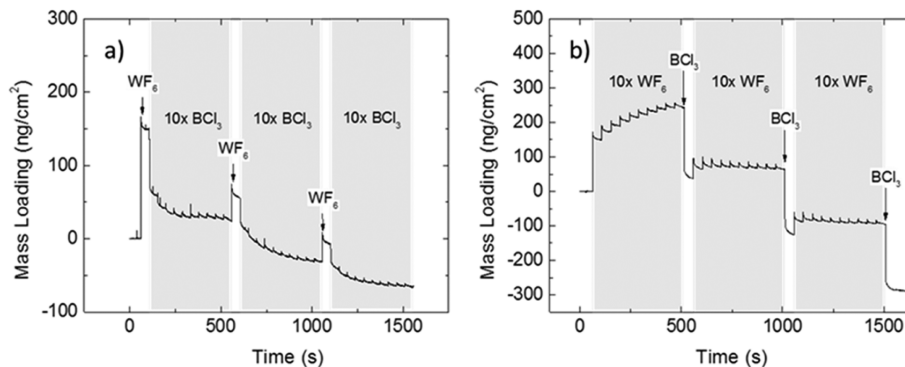


**Figure 14.** Saturation study of WF<sub>6</sub>/BCl<sub>3</sub> ALE process at 170 °C using QCM: (a) 1 WF<sub>6</sub> dose of 0.2 s per 10 BCl<sub>3</sub> doses of 0.2 s each and (b) 10 WF<sub>6</sub> doses of 0.1 s each per 1 BCl<sub>3</sub> dose of 1.0 s.

12. In this experiment, the QCM crystal was exposed to more than 100 cycles of TiO<sub>2</sub> or Al<sub>2</sub>O<sub>3</sub> ALD at 170 °C, followed immediately by WF<sub>6</sub>/BCl<sub>3</sub> etching. For TiO<sub>2</sub>, data in Figure 12 (repeated from Figure 10) show linear mass loss during WF<sub>6</sub>/BCl<sub>3</sub> exposures, consistent with ALE. For Al<sub>2</sub>O<sub>3</sub>, however, no etching is observed. As in Figure 2, the first WF<sub>6</sub> exposure leads to mass gain, but the mass does not change substantially during subsequent WF<sub>6</sub> and BCl<sub>3</sub> exposures. This result is consistent with the thermodynamic analysis where WF<sub>6</sub> reacts with Al<sub>2</sub>O<sub>3</sub> to form a solid passivating AlF<sub>3</sub> surface layer, which will not react with BCl<sub>3</sub> to form volatile AlCl<sub>3</sub>.<sup>20</sup>

**Self-Limiting Behavior of WF<sub>6</sub>/BCl<sub>3</sub> ALE.** To determine if WF<sub>6</sub>/BCl<sub>3</sub> etching of TiO<sub>2</sub> proceeds through self-limiting reactions, Figure 13 shows results of experiments at 170 °C in the ALE reactor on predeposited TiO<sub>2</sub> films where the change in film thickness was measured by ellipsometry after different extents of WF<sub>6</sub> or BCl<sub>3</sub> dosing. For these tests, we first deposited 100 cycles of ALD TiO<sub>2</sub> (~45 Å) on a set of samples and removed them from the ALD reactor. Individual samples were then exposed to 50 cycles of ALE under different exposure conditions, and the etch rate was determined by ellipsometry. Keeping the WF<sub>6</sub> exposure at 0.2 s, increasing the BCl<sub>3</sub> exposure to 1 s or larger showed etch saturation at ~0.6–0.7 Å/cycle. Similarly, keeping the BCl<sub>3</sub> exposure fixed at 1 s, the etch rate saturated with a WF<sub>6</sub> exposure greater than ~0.2 s/cycle. These etch rate values correspond to the average steady-state etch rate and are consistent with the QCM results in Figure 10b showing the steady-state etch rate is somewhat larger than the ALD growth rate per cycle.

The saturation behavior for the WF<sub>6</sub>/BCl<sub>3</sub> ALE process was further assessed with QCM, and data are given in Figure 14. It

is important to note that whereas the ellipsometry results in Figure 13 show the average steady-state etch rates, the QCM data in Figure 14 were collected during the first few ALE cycles immediately after ALD. We find that, under self-limiting saturated conditions, *vide infra*, the initial etch rates can be different from those determined during steady-state ALE. For the data in Figure 14a, a fresh ALD TiO<sub>2</sub> surface was exposed to 0.2 s of WF<sub>6</sub> followed by 10 BCl<sub>3</sub> subdoses of 0.2 s each. The WF<sub>6</sub> produced a mass gain followed by mass loss during the BCl<sub>3</sub> step. After the first WF<sub>6</sub> dose, the mass loss during BCl<sub>3</sub> saturates after 3 or 4 subdoses. After the second and third WF<sub>6</sub> doses, saturation is achieved within 10 BCl<sub>3</sub> subdoses, demonstrating self-limiting etching in the BCl<sub>3</sub> step. This condition corresponds to WF<sub>6</sub>/BCl<sub>3</sub> = 0.2/1.0 s, which is consistent with saturation conditions in Figure 13.

Likewise, Figure 14b shows results when a fresh TiO<sub>2</sub> surface is exposed to 10 WF<sub>6</sub> subdoses of 0.1 s each, followed by 1.0 s of BCl<sub>3</sub>. On the fresh TiO<sub>2</sub> surface, the first WF<sub>6</sub> dose leads to a relatively large mass gain followed by mass loss during the BCl<sub>3</sub> dose. In the second cycle, the first WF<sub>6</sub> subdose shows a much smaller mass gain, and subsequent WF<sub>6</sub> subdoses lead to no net mass change, indicating WF<sub>6</sub> reaction saturation. The overall dose conditions correspond to WF<sub>6</sub>/BCl<sub>3</sub> = 1.0/1.0 s. This is also consistent with saturation in Figure 13, but the net 1.0 s WF<sub>6</sub> dose/cycle substantially exceeds the 0.1–0.2 s/cycle required for steady-state saturation. This excess WF<sub>6</sub> leads to a different etch rate during the first few ALE cycles than that measured at steady state, but the overall reaction remains self-limiting. The ellipsometry (at steady state) and QCM analysis (during initial etch cycles) both confirm that the WF<sub>6</sub>/BCl<sub>3</sub> reaction sequence gives rise to self-limiting etching half-

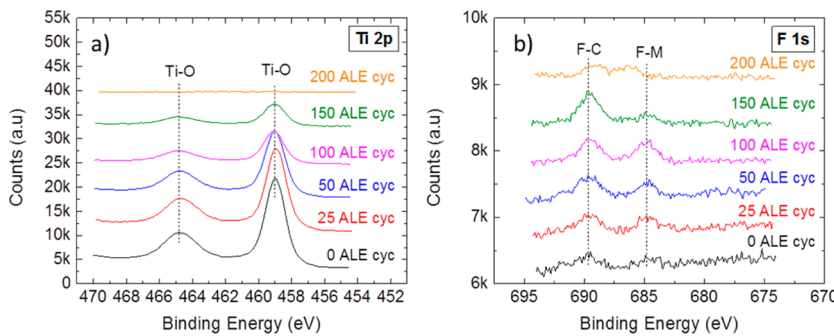


**Figure 15.** High resolution XPS scans of (a) Ti 2p and (b) F 1s regions for 4 nm  $\text{TiO}_2$  film following 0, 25, 50, 100, 150, and 200  $\text{WF}_6/\text{BCl}_3$  cycles in the ALE reactor at 170 °C.

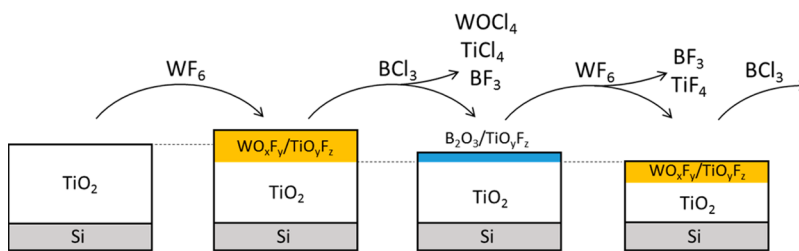


**Figure 16.** Schematic diagram describing the proposed etch mechanism for the  $\text{TiO}_2$  ALE process using  $\text{WF}_6$  and  $\text{BCl}_3$  at 170 °C: (1)  $\text{WF}_6$  adsorbs on the thick  $\text{TiO}_2$  surface, forming surface-bound  $\text{TiO}_y\text{F}_z$  and  $\text{WO}_x\text{F}_y$ . (2)  $\text{BCl}_3$  volatilizes the surface metal oxy fluoride species, forming  $\text{TiCl}_4$ ,  $\text{WCl}_4$ , and  $\text{BF}_3$ .

reactions, thereby validating that the process follows a thermal ALE sequence.

**Mass Uptake and Etch Rates during Initial  $\text{WF}_6/\text{BCl}_3$  Exposures versus Steady-State ALE.** In the CVE experiments at 220 °C shown in Figure 1, we noted that the mass gain during the first  $\text{WF}_6$  exposure was larger than that during subsequent dose steps. The QCM results in Figures 12 and 14 for the  $\text{WF}_6/\text{BCl}_3$  process show the  $\text{WF}_6$  mass uptake is also larger during the first dose than during the steady state ALE process. In this case, the mass loss during the first  $\text{BCl}_3$  dose is also larger than at steady state. The differences between the initial and the steady state behavior reflects differences in the surface condition. On the fresh  $\text{TiO}_2$  surface, the  $\text{WF}_6$  will react readily to yield surface tungsten oxides and fluorine that diffuse into the film. During steady-state etching, however, some of the  $\text{WF}_6$  is also consumed to volatilize surface boron oxide, creating a more well-defined etch rate per cycle. The different reactions and reaction rates during the first cycles will lead to ALE rate transitions, where the etch rate during early cycles could be faster or slower than at steady state.

It is interesting to note that rate evolution during ALE can be viewed as physically analogous to growth incubation commonly observed in ALD. Delayed nucleation in ALD occurs when the ALD precursors react differently on the growth substrate than on the growth surface. Likewise, in ALE, it is reasonable to expect the etch reactants will react differently with the fresh material being etched, i.e., the “etch substrate”, compared to the “etch surface”, i.e., the surface that is present following multiple etch cycles. This suggests, therefore, that early ALE rate inhibition or enhancement is a general phenomenon in thermal ALE processes, not limited to the  $\text{WF}_6/\text{BCl}_3$  process. Likewise, like growth incubation in ALD, the ALE rate transitions are expected to depend on the material being etched, the etch reactants, the process temperature, reactor wall preparation, and other conditions. Regarding reactor wall preparation, the

data presented here were generally collected after preparing our isothermal hot-wall reactor surface with ALD metal oxide. In our reactors, we noted that the ALE rate could be reduced when a series of ALE runs was performed in sequence, possibly resulting from excess boron oxide present on the reactor walls. We found performing a long  $\text{WF}_6$  exposure to remove boron oxide in the ALE chamber before loading samples acted to mitigate the effect.

**Analysis of  $\text{WF}_6/\text{BCl}_3$  ALE by XPS.** The  $\text{WF}_6/\text{BCl}_3$  ALE etching process was further characterized using XPS. For this data, a set of recently deposited  $\text{TiO}_2$  samples were etched with different numbers of  $\text{WF}_6/\text{BCl}_3$  ALE cycles and then removed from the reactor for analysis. Figure 15a shows that the intensity of the Ti 2p signal decreases with increasing number of  $\text{WF}_6/\text{BCl}_3$  ALE cycles, consistent with film etching. Figure 15b shows the F 1s signal under the same conditions. The peaks near 685 and 690 eV are assigned to fluorine bound to metal and carbon, respectively,<sup>53</sup> indicating metal fluorides and trace organic fluorine on the  $\text{TiO}_2$  surface. The metal fluorides are consistent with the expected ALE reactions. The organic fluorides are ascribed to reaction with adventitious carbon during sample transfer. Furthermore, the boron, chlorine, and tungsten content are also below the XPS detection limit. After 200 ALE cycles, the Ti 2p signal is below the detection limit confirming that the  $\text{TiO}_2$  film was completely etched, leaving trace amounts of halogen on the Si substrate surface.

**Schematic of the  $\text{WF}_6/\text{BCl}_3$  ALE Reaction Process.** Figure 16 shows a schematic for the proposed  $\text{WF}_6/\text{BCl}_3$  ALE reaction sequence consistent with the thermodynamic modeling, as well as the QCM, ellipsometry, and XPS data. First, like the chemical vapor etching mechanism, the initial  $\text{WF}_6$  adsorbs and fluorinates the  $\text{TiO}_2$  surface producing solid  $\text{WO}_x\text{F}_y$  and  $\text{TiO}_y\text{F}_z$ . This is shown in the XPS results in Figure 4, as well as QCM in Figures 10 and 12. At  $T < 200$  °C, the solid  $\text{WO}_x\text{F}_y$  layer is not sufficiently volatile to allow CVE.

After  $\text{WF}_6$ , the subsequent  $\text{BCl}_3$  exposure then leads to ligand exchange<sup>43</sup> yielding volatile  $\text{TiCl}_4$  and  $\text{WOCl}_4$ , as indicated by equilibrium thermodynamics in Figure 12. Thermodynamic models also suggest solid  $\text{B}_2\text{O}_3$  is a surface product. However, XPS analysis after  $\text{BCl}_3$  exposure showed no evidence for surface boron. The lack of B signal is expected because the samples are transferred in air for XPS, allowing surface  $\text{B}_2\text{O}_3$  to react with ambient moisture to form volatile boric acid,  $\text{H}_3\text{BO}_3$ .<sup>54</sup> The XPS data in Figure 15 show that, after  $\text{BCl}_3$  exposure, some fluorine remains on the  $\text{TiO}_2$  surface, denoted as  $\text{TiO}_y\text{F}_z$ . Also during the  $\text{BCl}_3$  exposure step at 170 °C,  $\text{BCl}_3$  is expected to react with  $\text{TiO}_2$  to form  $\text{TiCl}_4$  and  $\text{B}_2\text{O}_3$  ( $\Delta G = -109 \text{ kJ/mol TiO}_2$ ). The solid  $\text{B}_2\text{O}_3$  passivates the  $\text{TiO}_2$  surface, thereby self-limiting the  $\text{BCl}_3$  etching.

After  $\text{BCl}_3$ , the subsequent  $\text{WF}_6$  exposure reacts with  $\text{B}_2\text{O}_3$  to form volatile  $\text{BF}_3$  and  $\text{TiF}_4$ , and surface  $\text{WO}_3$ ,  $\text{WO}_x\text{F}_y$  and  $\text{TiO}_y\text{F}_z$ . Some surface  $\text{TiO}_y\text{F}_z$  is present from previous cycles, and this impedes fluorine diffusion,<sup>20–23,49,50</sup> thereby leading to less  $\text{WF}_6$  reaction than on fresh  $\text{TiO}_2$ . Upon establishing steady-state conditions, the  $\text{WF}_6/\text{BCl}_3$  atomic layer etch sequence continues until the  $\text{TiO}_2$  film is consumed. As shown in Figure 15, after 200 ALE cycles, no evidence for Ti 2p is observed by XPS. Moreover, the silicon substrate remaining after ALE shows a relatively small F 1s signal, indicating this ALE sequence leaves a clean surface after etching.<sup>29</sup>

## SUMMARY AND CONCLUSIONS

In this article, we demonstrated and described mechanisms for thermally driven selective chemical vapor etching (CVE) of  $\text{TiO}_2$  using  $\text{WF}_6$  at  $T > 200$  °C and selective atomic layer etching (ALE) of  $\text{TiO}_2$  using  $\text{WF}_6/\text{BCl}_3$  reactant exposures at  $T < 190$  °C. Other reactants, including  $\text{WF}_6/\text{Sn}(\text{acac})_2$ , also provided routes for low-temperature ALE. Using XPS and ellipsometry analysis, we physically confirm  $\text{TiO}_2$  etching and provide evidence that etching proceeds through  $\text{TiO}_2$  fluorination and formation of a low density  $\text{WO}_x\text{F}_y$  region. We also showed that the chemical selectively for etching of  $\text{TiO}_2$  over other oxides including  $\text{Al}_2\text{O}_3$  is due to the relative volatility of the metal fluoride product species.

For etching of  $\text{TiO}_2$  using  $\text{WF}_6$  and  $\text{BCl}_3$ , modeling confirms that the process proceeds through two complementary thermodynamically favorable half-reaction steps, indicating creation of volatile  $\text{TiCl}_4$ ,  $\text{BF}_3$ , and  $\text{WOCl}_4$ . Film thickness measurements after etching under a range of exposure conditions confirm steady-state self-limiting etch saturation, confirming thermal atomic layer etching, with an etch rate of ~0.6–0.7 Å/cycle at 170 °C. At slightly lower temperatures, between 130° and 150 °C, the process is more temperature independent, with an etch rate of ~0.3 Å/cycle. We show that the ALE process is selective for etching  $\text{TiO}_2$  over  $\text{Al}_2\text{O}_3$ , and modeling further suggests this process will be favorable for ALE of  $\text{HfO}_2$  and  $\text{ZrO}_2$ . Analysis by XPS shows complete removal of  $\text{TiO}_2$  films on silicon, resulting in a clean substrate with trace amounts of surface fluorination. We also describe and demonstrate how the rate of ALE during initial etch cycles may be different from that observed at steady state, and we conclude that rate evolution during initiation of thermal ALE may be a general phenomenon that is physically analogous to well-known rate transitions during substrate-dependent nucleation in ALD.

## AUTHOR INFORMATION

### Corresponding Author

(G.N.P.) E-mail: [gnp@ncsu.edu](mailto:gnp@ncsu.edu).

### ORCID

Paul C. Lemaire: [0000-0002-2077-8114](https://orcid.org/0000-0002-2077-8114)

Gregory N. Parsons: [0000-0002-0048-5859](https://orcid.org/0000-0002-0048-5859)

### Author Contributions

All authors have given approval to the final version of the manuscript.

### Notes

The authors declare no competing financial interest.

## ACKNOWLEDGMENTS

The authors acknowledge support from Lam Research and EMD Performance Materials. They also acknowledge the use of the Analytical Instrumentation Facility (AIF) at North Carolina State University, which is supported by the State of North Carolina and the National Science Foundation.

## REFERENCES

- Trucks, G. W.; Raghavachari, K.; Higashi, G. S.; Chabal, Y. C. Mechanism of HF Etching of Silicon Surfaces: A Theoretical Understanding of Hydrogen Passivation. *Phys. Rev. Lett.* **1990**, *65*, 504–507.
- Kang, J. K.; Musgrave, C. B. The Mechanism of HF/H<sub>2</sub>O Chemical Etching of SiO<sub>2</sub>. *J. Chem. Phys.* **2002**, *116*, 275.
- Hoshino, T.; Nishioka, Y. Etching Process of SiO<sub>2</sub> by HF Molecules. *J. Chem. Phys.* **1999**, *111*, 2109.
- Ritala, M. Atomic Layer Deposition of Oxide Thin Films with Metal Alkoxides as Oxygen Sources. *Science (Washington, DC, U. S.)* **2000**, *288*, 319–321.
- Atanasov, S. E.; Kalanyan, B.; Parsons, G. N. Inherent Substrate-Dependent Growth Initiation and Selective-Area Atomic Layer Deposition of TiO<sub>2</sub> Using “water-Free” Metal-Halide/metal Alkoxide Reactants. *J. Vac. Sci. Technol., A* **2016**, *34*, 01A148.
- Liu, J.; Lennard, W. N.; Goncharova, L. V.; Landheer, D.; Wu, X.; Rushworth, S. A.; Jones, A. C. Atomic Layer Deposition of Hafnium Silicate Thin Films Using Tetrakis(diethylamido)hafnium and Tris(2-Methyl-2-Butoxy)silanol. *J. Electrochem. Soc.* **2009**, *156*, G89.
- Frank, M. M.; Chabal, Y. J.; Green, M. L.; Delabie, A.; Brijs, B.; Wilk, G. D.; Ho, M.-Y.; da Rosa, E. B. O.; Baumvol, I. J. R.; Stedile, F. C. Enhanced Initial Growth of Atomic-Layer-Deposited Metal Oxides on Hydrogen-Terminated Silicon. *Appl. Phys. Lett.* **2003**, *83*, 740.
- Chaukulkar, R. P.; Agarwal, S. Atomic Layer Deposition of Titanium Dioxide Using Titanium Tetrachloride and Titanium Tetraisopropoxide as Precursors. *J. Vac. Sci. Technol., A* **2013**, *31*, 031509.
- Park, K. J.; Terry, D. B.; Stewart, S. M.; Parsons, G. N. In Situ Auger Electron Spectroscopy Study of Atomic Layer Deposition: Growth Initiation and Interface Formation Reactions during Ruthenium ALD on Si-H, SiO<sub>2</sub>, and HfO<sub>2</sub> Surfaces. *Langmuir* **2007**, *23*, 6106–6112.
- Holmes, P. J.; Snell, J. E. A Vapour Etching Technique for the Photolithography of Silicon Dioxide. *Microelectron. Reliab.* **1966**, *5*, 337–341.
- McIntosh, R.; Kuan, T.-S.; Defresart, E. Hydrogen Fluoride Vapor Etching for Pre-Epi Silicon Surface Preparation. *J. Electron. Mater.* **1992**, *21*, 57–60.
- Helms, C. R.; Deal, B. E. Mechanisms of the HF/H<sub>2</sub>O Vapor Phase Etching of SiO<sub>2</sub>. *J. Vac. Sci. Technol., A* **1992**, *10*, 806.
- Miki, N.; Kikuyama, H.; Kawanabe, I.; Miyashita, M.; Ohmi, T. Gas-Phase Selective Etching of Native Oxide. *IEEE Trans. Electron Devices* **1990**, *37*, 107–115.
- Lee, Y.; Sun, H.; Young, M. J.; George, S. M. Atomic Layer Deposition of Metal Fluorides Using HF-Pyridine as the Fluorine Precursor. *Chem. Mater.* **2016**, *28*, 2022.

- (15) Oehrlein, G. S.; Metzler, D.; Li, C. Atomic Layer Etching at the Tipping Point: An Overview. *ECS J. Solid State Sci. Technol.* **2015**, *4*, N5041–N5053.
- (16) Kanarik, K. J.; Lill, T.; Hudson, E. A.; Sriraman, S.; Tan, S.; Marks, J.; Vahedi, V.; Gottscho, R. A. Overview of Atomic Layer Etching in the Semiconductor Industry. *J. Vac. Sci. Technol., A* **2015**, *33*, 020802.
- (17) Faraz, T.; Roozeboom, F.; Knoops, H. C. M.; Kessels, W. M. M. Atomic Layer Etching: What Can We Learn from Atomic Layer Deposition? *ECS J. Solid State Sci. Technol.* **2015**, *4*, N5023–N5032.
- (18) Carver, C. T.; Plombon, J. J.; Romero, P. E.; Suri, S.; Tronic, T. A.; Turkot, R. B., Jr. Atomic Layer Etching: An Industry Perspective. *ECS J. Solid State Sci. Technol.* **2015**, *4*, N5005–N5009.
- (19) George, S. M.; Lee, Y. Prospects for Thermal Atomic Layer Etching Using Sequential, Self-Limiting Fluorination and Ligand-Exchange Reactions. *ACS Nano* **2016**, *10*, 4889–4894.
- (20) Lee, Y.; Huffman, C.; George, S. M. Selectivity in Thermal Atomic Layer Etching Using Sequential, Self-Limiting Fluorination and Ligand-Exchange Reactions. *Chem. Mater.* **2016**, *28*, 7657.
- (21) Lee, Y.; George, S. M. Atomic Layer Etching of Al<sub>2</sub>O<sub>3</sub> Using Sequential, Self-Limiting Thermal Reactions with Sn(acac)<sub>2</sub> and Hydrogen Fluoride. *ACS Nano* **2015**, *9*, 2061–2070.
- (22) Lee, Y.; DuMont, J. W.; George, S. M. Mechanism of Thermal Al<sub>2</sub>O<sub>3</sub> Atomic Layer Etching Using Sequential Reactions with Sn(acac)<sub>2</sub> and HF. *Chem. Mater.* **2015**, *27*, 3648–3657.
- (23) Lee, Y.; DuMont, J. W.; George, S. M. Trimethylaluminum as the Metal Precursor for the Atomic Layer Etching of Al<sub>2</sub>O<sub>3</sub> Using Sequential, Self-Limiting Thermal Reactions. *Chem. Mater.* **2016**, *28*, 2994–3003.
- (24) Lee, Y.; DuMont, J. W.; George, S. M. Atomic Layer Etching of HfO<sub>2</sub> Using Sequential, Self-Limiting Thermal Reactions with Sn(acac)<sub>2</sub> and HF. *ECS J. Solid State Sci. Technol.* **2015**, *4*, N5013–N5022.
- (25) Droes, S. R.; Kodas, T. T.; Hampden-Smith, M. J. Etching of ZnO Films with Hexafluoroacetyleacetone. *Adv. Mater.* **1998**, *10*, 1129–1133.
- (26) Steger, R.; Masel, R. Chemical Vapor Etching of Copper Using Oxygen and 1,1,1,5,5-Hexafluoro-2,4-Pentanedione. *Thin Solid Films* **1999**, *342*, 221–229.
- (27) Jain, A.; Kodas, T. T.; Hampden-Smith, M. J. Thermal Dry-Etching of Copper Using Hydrogen Peroxide and Hexafluoroacetyleacetone. *Thin Solid Films* **1995**, *269*, 51–56.
- (28) Min, K. S.; Kang, S. H.; Kim, J. K.; Jhon, Y. I.; Jhon, M. S.; Yeom, G. Y. Atomic Layer Etching of Al<sub>2</sub>O<sub>3</sub> Using BC<sub>13</sub>/Ar for the Interface Passivation Layer of III–V MOS Devices. *Microelectron. Eng.* **2013**, *110*, 457–460.
- (29) Ikeda, K.; Imai, S.; Matsumura, M. Atomic Layer Etching of Germanium. *Appl. Surf. Sci.* **1997**, *112*, 87–91.
- (30) O'Donnell, T. A.; Stewart, D. F. Reactivity of Transition Metal Fluorides. I. Higher Fluorides of Chromium, Molybdenum, and Tungsten. *Inorg. Chem.* **1966**, *5*, 1434–1437.
- (31) Koutsospyros, A.; Braida, W.; Dermatas, D.; Strigul, N.; Christodoulatos, C. A Review of Tungsten: From Environmental Obscurity to Scrutiny. *J. Hazard. Mater.* **2006**, *136*, 1–19.
- (32) Kobayashi, N.; Nakamura, Y.; Goto, H.; Homma, Y. In Situ Infrared Reflection and Transmission Absorption Spectroscopy Study of Surface Reactions in Selective Chemical-Vapor Deposition of Tungsten Using WF<sub>6</sub> and SiH<sub>4</sub>. *J. Appl. Phys.* **1993**, *73*, 4637.
- (33) Tägtström, P. Atomic Layer Epitaxy of Tungsten Oxide Films Using Oxyfluorides as Metal Precursors. *J. Electrochem. Soc.* **1999**, *146*, 3139.
- (34) Knapas, K.; Rahtu, A.; Ritala, M. Etching of Nb<sub>2</sub>O<sub>5</sub> Thin Films by NbCl<sub>5</sub>. *Chem. Vap. Deposition* **2009**, *15*, 269–273.
- (35) Kalanyan, B.; Lemaire, P. C.; Atanasov, S. E.; Ritz, M. J.; Parsons, G. N. Using Hydrogen To Expand the Inherent Substrate Selectivity Window During Tungsten Atomic Layer Deposition. *Chem. Mater.* **2016**, *28*, 117–126.
- (36) Kalanyan, B.; Losego, M. D.; Oldham, C. J.; Parsons, G. N. Low-Temperature Atomic Layer Deposition of Tungsten Using Tungsten Hexafluoride and Highly-Diluted Silane in Argon. *Chem. Vap. Deposition* **2013**, *19*, 161–166.
- (37) Powell, C. J.; Jablonski, A. NIST Standard Reference Database 82; 2011.
- (38) Fuentes, G. G.; Elizalde, E.; Yubero, F.; Sanz, J. M. Electron Inelastic Mean Free Path for Ti, TiC, TiN and TiO<sub>2</sub> as Determined by Quantitative Reflection Electron Energy-Loss Spectroscopy. *Surf. Interface Anal.* **2002**, *33*, 230–237.
- (39) Vasilopoulou, M.; Kostis, I.; Vourdas, N.; Papadimitropoulos, G.; Douvas, A.; Boukos, N.; Kennou, S.; Davazoglou, D. Influence of the Oxygen Substoichiometry and of the Hydrogen Incorporation on the Electronic Band Structure of Amorphous Tungsten Oxide Films. *J. Phys. Chem. C* **2014**, *118*, 12632–12641.
- (40) Mouat, A. R.; Mane, A. U.; Elam, J. W.; Delferro, M.; Marks, T. J.; Stair, P. C. Volatile Hexavalent Oxo-Amidinate Complexes: Molybdenum and Tungsten Precursors for Atomic Layer Deposition. *Chem. Mater.* **2016**, *28*, 1907–1919.
- (41) Lee, Y.; DuMont, J. W.; George, S. M. Atomic Layer Etching of AlF<sub>3</sub> Using Sequential, Self-Limiting Thermal Reactions with Sn(acac)<sub>2</sub> and Hydrogen Fluoride. *J. Phys. Chem. C* **2015**, *119*, 25385–25393.
- (42) Ramanath, G.; Greene, J. E.; Carlsson, J. R. A.; Allen, L. H.; Hornback, V. C.; Allman, D. J. W. Deposition Titanium Fluoride-Formation during WF<sub>6</sub> Reduction by Ti: Reaction Path and Mechanisms. *J. Appl. Phys.* **1999**, *85*, 1961.
- (43) Fracassi, F.; d'Agostino, R. Chemistry of Titanium Dry Etching in Fluorinated and Chlorinated Gases. *Pure Appl. Chem.* **1992**, *64*, 703–707.
- (44) Lemaire, P. C.; King, M.; Parsons, G. N. Understanding Inherent Substrate Selectivity during Atomic Layer Deposition: Effect of Surface Preparation, Hydroxyl Density, and Metal Oxide Composition on Nucleation Mechanisms during Tungsten ALD. *J. Chem. Phys.* **2017**, *146*, 052811.
- (45) Bestwick, T. D.; Oehrlein, G. S. Tungsten Etching Mechanisms in CF<sub>4</sub>/O<sub>2</sub> Reactive Ion Etching Plasmas. *J. Appl. Phys.* **1989**, *66*, 5034.
- (46) Lee, Y. J.; Park, C.-O.; Kim, D.-W.; Chun, J. S. The Effects of Deposition Temperature on the Interfacial Properties of SiH<sub>4</sub> Reduced Blanket Tungsten on TiN Glue Layer. *J. Electron. Mater.* **1994**, *23*, 1075–1080.
- (47) Louvain, N.; Karkar, Z.; El-Ghazzi, M.; Bonnet, P.; Guérin, K.; Willmann, P. Fluorination of Anatase TiO<sub>2</sub> towards Titanium Oxyfluoride TiOF<sub>2</sub>: A Novel Synthesis Approach and Proof of the Li-Insertion Mechanism. *J. Mater. Chem. A* **2014**, *2*, 15308.
- (48) Baxter, D. V.; Chisolm, M. H.; Doherty, S.; Gruhn, N. E. Chemical Vapour Deposition of Electrochromic Tungsten Oxide Films Employing Volatile tungsten(VI) Oxo Alkoxide/-Diketonate Complexes. *Chem. Commun.* **1996**, 1129.
- (49) Ortega, Y.; Lamiel-Garcia, O.; Hevia, D. F.; Tosoni, S.; Oviedo, J.; San-Miguel, M. A.; Illas, F. Theoretical Study of the Fluorine Doped Anatase Surfaces. *Surf. Sci.* **2013**, *618*, 154–158.
- (50) Tosoni, S.; Lamiel-Garcia, O.; Fernandez Hevia, D.; Illas, F. Theoretical Study of Atomic Fluorine Diffusion through Bulk TiO<sub>2</sub> Polymorphs. *J. Phys. Chem. C* **2013**, *117*, 5855–5860.
- (51) Mäntymäki, M.; Heikkilä, M. J.; Puukilainen, E.; Mizohata, K.; Marchand, B.; Räisänen, J.; Ritala, M.; Leskelä, M. Atomic Layer Deposition of AlF<sub>3</sub> Thin Films Using Halide Precursors. *Chem. Mater.* **2015**, *27*, 604–611.
- (52) Pilvi, T.; Puukilainen, E.; Munnik, F.; Leskelä, M.; Ritala, M. ALD of YF<sub>3</sub> Thin Films from TiF<sub>4</sub> and Y(thd)<sub>3</sub> Precursors. *Chem. Vap. Deposition* **2009**, *15*, 27–32.
- (53) Thermo Scientific XPS: Fluorine. <http://xpssimplified.com/elements/fluorine.php> (accessed May 28, 2017).
- (54) Putkonen, M.; Niinistö, L. Atomic Layer Deposition of B<sub>2</sub>O<sub>3</sub> Thin Films at Room Temperature. *Thin Solid Films* **2006**, *514*, 145–149.